Icarus 199 (2009) 295–302

Contents lists available at ScienceDirect

Icarus

www.elsevier.com/locate/icarus

Shallow radar (SHARAD) sounding observations of the Medusae Fossae Formation, Mars

Lynn M. Carter [a,*], Bruce A. Campbell [a], Thomas R. Watters [a], Roger J. Phillips [b], Nathaniel E. Putzig [b], Ali Safaeinili [c], Jeffrey J. Plaut [c], Chris H. Okubo [d], Anthony F. Egan [b], Roberto Seu [e], Daniela Biccari [e], Roberto Orosei [f]

[a] Smithsonian Institution, Center for Earth and Planetary Studies, MRC 315, PO Box 37012, Washington, DC 20013-7012, USA
[b] Southwest Research Institute, 1050 Walnut St., Suite 300, Boulder, CO 80302, USA
[c] Jet Propulsion Laboratory, 4800 Oak Grove Dr., Pasadena, CA 91109, USA
[d] U.S. Geological Survey, 2255 N. Gemini Dr., Flagstaff, AZ 86001, USA
[e] Dipartimento INFOCOM, Università di Roma "La Sapienza," I-00184 Rome, Italy
[f] Istituto di Astrofisica Spaziale e Fisica Cosmica, Istituto Nazionale di Astrofisica, I-00133 Rome, Italy

ARTICLE INFO

Article history:
Received 29 May 2008
Revised 18 September 2008
Accepted 2 October 2008
Available online 18 November 2008

Keywords:
Mars
Mars, surface
Radar observations
Volcanism

ABSTRACT

The SHARAD (shallow radar) sounding radar on the Mars Reconnaissance Orbiter detects subsurface reflections in the eastern and western parts of the Medusae Fossae Formation (MFF). The radar waves penetrate up to 580 m of the MFF and detect clear subsurface interfaces in two locations: west MFF between 150 and 155° E and east MFF between 209 and 213° E. Analysis of SHARAD radargrams suggests that the real part of the permittivity is ~3.0, which falls within the range of permittivity values inferred from MARSIS data for thicker parts of the MFF. The SHARAD data cannot uniquely determine the composition of the MFF material, but the low permittivity implies that the upper few hundred meters of the MFF material has a high porosity. One possibility is that the MFF is comprised of low-density welded or interlocked pyroclastic deposits that are capable of sustaining the steep-sided yardangs and ridges seen in imagery. The SHARAD surface echo power across the MFF is low relative to typical martian plains, and completely disappears in parts of the east MFF that correspond to the radar-dark Stealth region. These areas are extremely rough at centimeter to meter scales, and the lack of echo power is most likely due to a combination of surface roughness and a low near-surface permittivity that reduces the echo strength from any locally flat regions. There is also no radar evidence for internal layering in any of the SHARAD data for the MFF, despite the fact that tens-of-meters scale layering is apparent in infrared and visible wavelength images of nearby areas. These interfaces may not be detected in SHARAD data if their permittivity contrasts are low, or if the layers are discontinuous. The lack of closely spaced internal radar reflectors suggests that the MFF is not an equatorial analog to the current martian polar deposits, which show clear evidence of multiple internal layers in SHARAD data.

1. Introduction

The Medusae Fossae Formation (MFF) stretches across the martian equator and parts of the northern hemisphere lowlands from ~140 to 240° E longitude. The surface of the MFF is dominated by wind erosion, with rough, parallel-grooved surfaces or yardangs present in most places (Hynek et al., 2003; Edgett and Malin, 2000). It is a geologically young deposit, overlying Amazonian-aged lava flows in the lowlands of Elysium Planitia and Noachian-aged cratered highlands along parts of the dichotomy boundary (Hynek et al., 2003; Bradley et al., 2002; Head and Kreslavsky, 2004). Exhumed and buried craters are common; towards the north, the formation is almost completely eroded to plains level (Hynek et al., 2003; Edgett and Malin, 2000). High-resolution images show slope streaks and small dune fields, which suggests that a fine-grained material probably makes up most of the deposit. Several hypotheses have been suggested to explain the origin of the MFF deposits, including pyroclastic density currents, volcanic fall deposits and ignimbrites (Hynek et al., 2003; Muhleman et al., 1991; Zimbelman et al., 1997), aeolian deposits (Tanaka, 2000), or relic polar layered deposits (Head and Kreslavsky, 2004; Schultz and Lutz, 1988).

The eastern parts of the MFF correspond to the radar-dark Stealth region identified in 3-cm and 13-cm ground-based radar images (Muhleman et al., 1991; Harmon et al., 1999). The darkest part of the Stealth region, which has no received echo power

* Corresponding author. Fax: +1 202 786 2612.
E-mail address: carterl@si.edu (L.M. Carter).

0019-1035/$ – see front matter
doi:10.1016/j.icarus.2008.10.007

above the noise level (Muhleman et al., 1991, 1995), is located southwest of Tharsis. The low radar backscatter suggests some combination of a low surface permittivity and few cm-scale and larger rocks (Muhleman et al., 1991; Harmon et al., 1999). The Stealth component of the MFF was inferred to be at least 5 m thick, although the radar could potentially penetrate up to several tens of meters in low electrical-loss material (Harmon et al., 1999; Muhleman et al., 1995). The terrain with the lowest radar backscatter is centered south of Olympus Mons, but the total area showing reduced radar reflectivity stretches across the equator from 140 to 240° E, and encompasses the entire longitudinal extent of the MFF (Edgett et al., 1997).

The surface properties and atmosphere of Mars are conducive to explosive volcanism. Models of martian vulcanian eruptions have shown that ash fall deposits may travel 25 km or more from the vent, depending on the wind strength and direction (Fagents and Wilson, 1996). Convective plumes from long-lived plinian eruptions can reach heights up to 20 km (Glaze and Baloga, 2002), and in this case the millimeter-sized clasts may travel a few kilometers to 20 km depending on the winds (Wilson and Head, 2007). Micron-sized particles may be carried farther by the wind (Wilson and Head, 2007). Possible sites of explosive volcanism and ash deposits on Mars include Alba Patera (Mouginis-Mark et al., 1988), Apollinaris Patera (Robinson et al., 1993), the summit of Arsia Mons (Mouginis-Mark, 2002) and Tyrrhena and Hadriaca Paterae (Greeley and Crown, 1990; Crown and Greeley, 1993). One unresolved problem with the volcanic origin hypothesis for the MFF is the lack of identified source regions, although it has been suggested that Tharsis-related volcanism was a major contributor (Hynek et al., 2003; Edgett and Malin, 2000). Ash from explosive eruptions can also potentially settle over a large area, leading to low-elevation constructs that are difficult to identify in images, and which can be easily buried by subsequent volcanism (Fagents and Wilson, 1996; Hynek et al., 2003; Tanaka et al., 2005).

If MFF is analogous to a polar layered deposit, its interior may be composed primarily of ice. Schultz and Lutz (1988) proposed that the MFF is comprised of relic polar layered deposits formed as a result of polar wandering. Head and Kreslavsky (2004) suggested that the MFF is a young, ice-rich deposit formed during recent periods of high obliquity. Both Schultz and Lutz (1988) and Head and Kreslavsky (2004) cite the presence of internal layering as well as the overall thickness and topography of the deposit as evidence that the MFF may be similar to martian polar layered terrain. However, Bradley et al. (2002) compared Mars Orbiter Laser Altimeter (MOLA) data and Mars Orbiter Camera (MOC) images of the poles with those of the MFF and concluded that the two terrains have very different characteristics, including differences in surface slopes, layer topography, and in the heights of ridges and valleys.

The MARSIS (Mars Advanced Radar for Subsurface and Ionospheric Sounding) instrument on the Mars Express orbiter has also been used to study the MFF (Watters et al., 2007). MARSIS operates at frequencies between 1.3 and 5.5 MHz, has a free space vertical resolution of 150 m, and can penetrate up to a few km in depth depending on the material (Picardi et al., 2005). MARSIS detects basal interfaces beneath most of the MFF, including in the regions of Gordii Dorsum, Amazonis Mensa, Eumenides Dorsum, Lucus Planum and the far western deposits south of Elysium Mons (Watters et al., 2007). Time-delay values measured from the MARSIS radargrams for deposits up to about 2.5 km in thickness correspond to a bulk real permittivity value of $\sim 2.9 \pm 0.4$ for the MFF material (Watters et al., 2007). The two most likely explanations for such a low permittivity are either a dry, low-density material such as volcanic ash, or an ice-rich material (Watters et al., 2007). If the MFF is composed mostly of dry ash, it must have a high porosity, even at km-scale depths.

The SHARAD radar sounding instrument on the Mars Reconnaissance Orbiter (MRO) is complementary to MARSIS: SHARAD has a higher resolution and is capable of detecting finely spaced interfaces at depths of up to 1000 m, but cannot penetrate as deeply. In this paper we discuss results from a SHARAD campaign to search for subsurface interfaces across the entire Medusae Fossae Formation. We summarize the SHARAD data products and the location of subsurface interfaces across the MFF, characterize the material properties of the deposit as inferred from SHARAD and MARSIS data, and, finally, discuss the correlation between SHARAD echoes and local geologic features.

2. Summary of SHARAD Medusae Fossae Formation observations

SHARAD operates at a center frequency of 20 MHz ($\lambda = 15$ m) with a 10 MHz bandwidth (Seu et al., 2004, 2007a). With a nominal vertical resolution of 15 m in free-space, and 5–10 m vertical resolution in common geologic materials, SHARAD is capable of discerning thin subsurface layers. The lateral resolution of SHARAD is 3 to 6 km, reducible to 300 to 1000 m in the along-track direction with synthetic aperture focusing (Seu et al., 2004, 2007a). For smooth surfaces, the cross-track resolution is ~750 m (Seu et al., 2007a). On the ground, the data are correlated with the radar chirp and spacecraft orbital information is used to determine the range relative to a topographic reference, in this case a biaxial ellipsoid with dimensions equal to the polar and equatorial radii of Mars. The SHARAD data are displayed as radargrams, with along-track distance on the x-axis and range-delay time increasing downward on the y-axis. The radargrams shown in this paper have been processed using a synthetic-aperture focusing algorithm to improve the signal-to-noise ratio of the subsurface reflectors under the rough MFF surface. Although the SHARAD processing algorithm will correct for the ionosphere based on the sun elevation angle (Safaeinili et al., 2007), all the data used here were acquired at night when ionospheric distortion is minimal, and in this case no correction is applied.

The SHARAD data are sensitive to wavelength-scale topographic features that contribute off-nadir surface clutter to the radargrams. MOLA topographic data do not have sufficient resolution to model all of the clutter sources seen by SHARAD, but they can be used to determine the effects of large-scale structures in the images. For each SHARAD ground-track, we produce a simulated radargram that can be compared with the observed radargram to identify clutter sources large enough to appear in the MOLA data. Radargrams projected to the surface along-track can also be compared with images to search for smaller clutter sources.

SHARAD has obtained radar tracks across the MFF from 140 to 230° E longitude, including the western portions south of Elysium Planitia, Apollinaris Patera, Lucus Planum, Eumenides Dorsum, Amazonis Mensa, and Gordii Dorsum. While the MARSIS radar detects the basal interface of the MFF along its entire longitudinal extent (Watters et al., 2007), SHARAD detects subsurface echoes only from the far eastern and western portions of the deposit. The central portion of the MFF, including both Lucus Planum and Apollinaris Patera, has a high surface roughness and the SHARAD radargrams are dominated by surface clutter from ridges and craters. With its longer wavelengths, MARSIS is both less susceptible to surface clutter and able to see deeper reflectors.

The western parts of the MFF consist of relatively low-relief lobes that extend from the dichotomy boundary onto the surrounding plains. Fig. 1 shows the western MFF with SHARAD ground tracks shown in red where there are subsurface echoes. Radargrams of some of these same orbits are shown in Fig. 2. In this part of the MFF, SHARAD sees through low-relief hills south

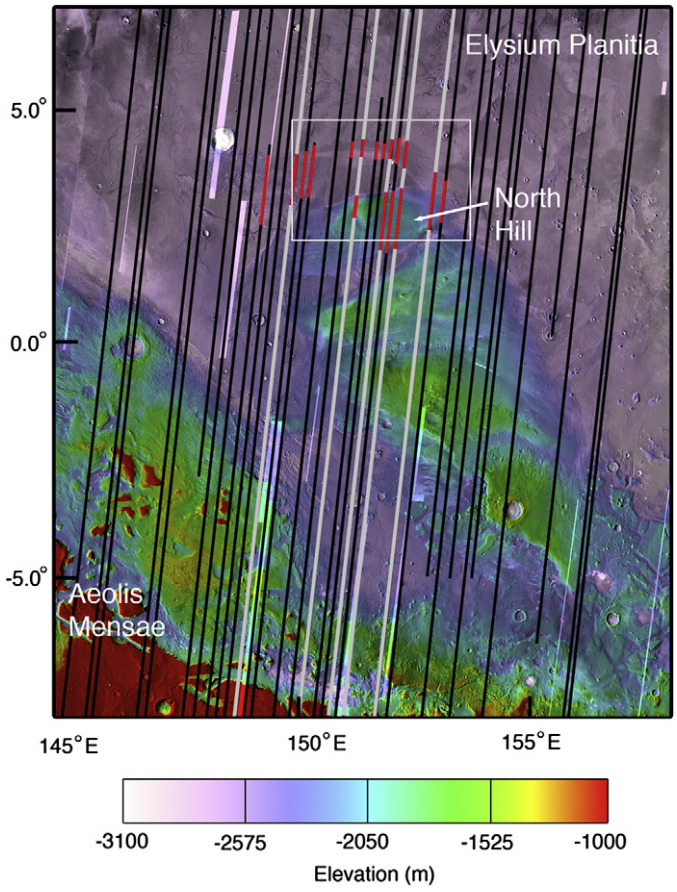

Fig. 1. SHARAD observation ground-tracks across the western part of MFF. The base map is THEMIS daytime infrared with color MOLA topography overlaid. The ground tracks are shown in red where SHARAD detects a subsurface interface beneath the MFF. Grey ground tracks correspond to observations shown in Fig. 2. Some available ground tracks were omitted for clarity, but adjacent observations show the same subsurface features. The location of the THEMIS image shown in Fig. 3 is indicated with a white box. Subsurface detections off the MFF in Elysium Planitia (north of the white box) are not marked with red lines in the image.

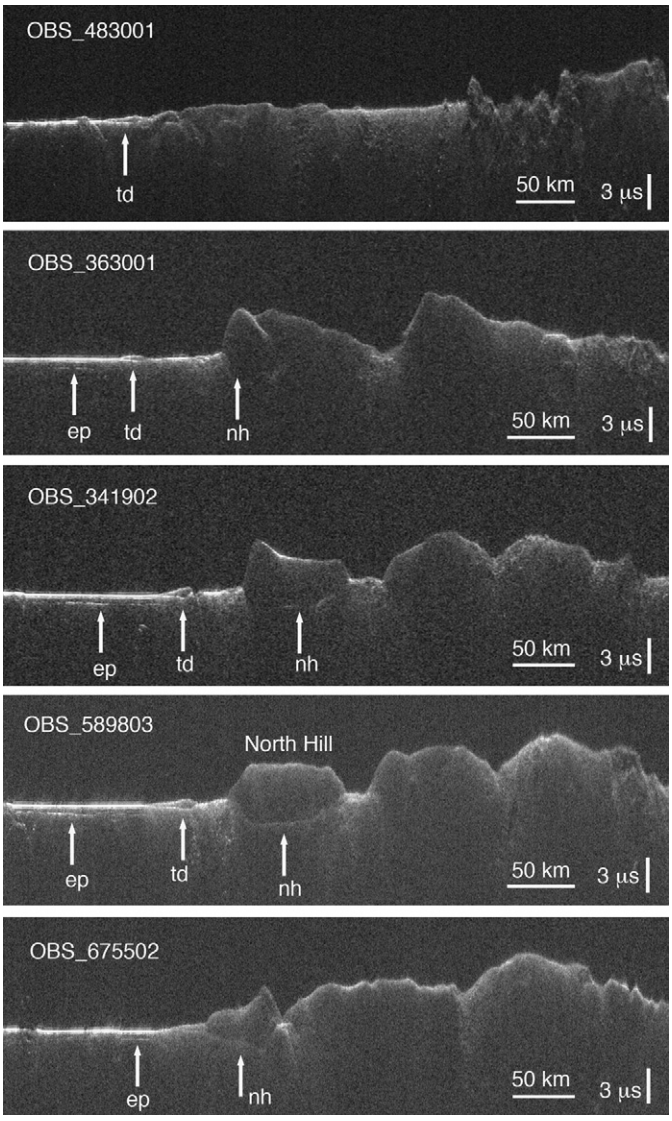

Fig. 2. SHARAD radargrams of deposits in west MFF. The radargrams are ordered from west (top) to east (bottom) and are shown with north to the left on each image. Ground-tracks are indicated in Fig. 1. Subsurface interfaces occur beneath thin 50–100 m deposits (arrows marked td) and beneath the ∼580 m North Hill (arrows marked nh). In some places, plains reflectors can be seen under Elysium Planitia (arrows marked ep). A scale bar for the time-delay values is shown on the far right of each radargram.

of Elysium Planitia and northeast of Aeolis Mensae. Watters et al. (2007) referred to the upper part of the lobe (shown in Fig. 1) as North Hill, and we repeat that nomenclature in this paper to avoid confusion. At a height of ∼580 m as measured from MOLA data, North Hill is the thickest part of the MFF for which SHARAD detects a subsurface interface. MARSIS detects both the subsurface interface beneath North Hill and an interface beneath a higher-elevation hill to the south that is apparently too thick for SHARAD to penetrate (Watters et al., 2007). Fig. 3 is a Mars Odyssey Thermal Emission Imaging System (THEMIS) daytime infrared image of the North Hill area (Christensen et al., 2004). The THEMIS image shows contrasts between the hills and the plains more clearly than available optical imagery. The radar-transparent hills to the north, marked as "thin deposits" in Fig. 3, are no more than 100 m thick.

The eastern part of the Medusae Fossae Formation lies southwest of Olympus Mons and includes large hills that are up to a few kilometers in elevation. Subsurface interfaces detected here by SHARAD occur primarily between Gordii Dorsum and Amazonis Mensa (Fig. 4). A subset of the corresponding radargrams is shown in Fig. 5, and it is clear that the MFF deposit thickens toward the east, from about 180 m to about 315 m. Further east, the lower interface is no longer detected by the radar, presumably as a result of signal attenuation in a thicker deposit. Depth estimates were derived from round-trip echo delay, assuming a real permittivity of 3. In the eastern part of the study region, MARSIS observations show subsurface interfaces at ∼340 and 730 m depth, again assuming a real permittivity of 3 (Watters et al., 2007). The SHARAD reflector at ∼315 m depth and the upper MARSIS reflector likely arise from the same subsurface interface. To the west of Amazonis Mensa, SHARAD detects a subsurface interface beneath relatively flat terrain near the dichotomy boundary (Fig. 4). In this area, the reflectors are about 60 m below the surface (assuming a permittivity of 3) and are most likely boundaries between very thin deposits of the MFF material and the underlying plains. Northwest of Gordii Dorsum SHARAD detects dipping subsurface reflectors similar to those mapped in central Amazonis Planitia by Campbell et al. (2008). These features occur underneath Late- to Mid-Amazonian period plains lava flows (labeled as AAa2s by Tanaka et al., 2005) and do not represent an interface with the MFF materials.

3. Physical properties of the Medusae Fossae Formation material

Sounding radar measurements can be used to estimate the complex permittivity ($\varepsilon' \pm i\varepsilon''$) of the MFF material. The real part of

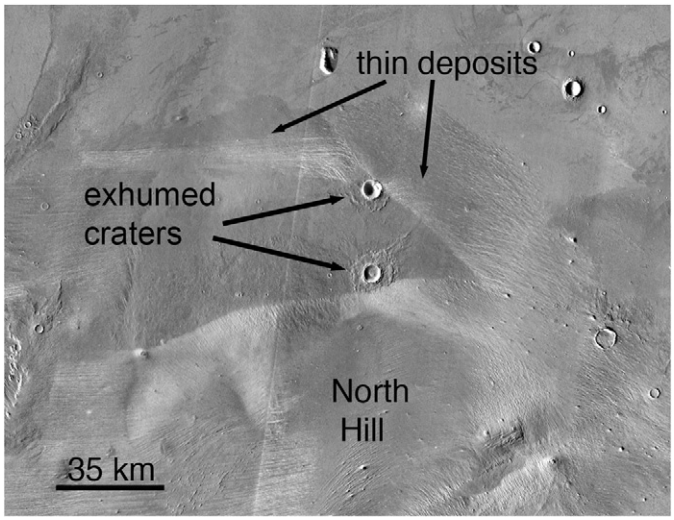

Fig. 3. THEMIS daytime infrared mosaicked image of low-relief hills in west MFF. Craters at the image center were emplaced on the underlying plains and are being exhumed in the area between the thin deposits and the feature marked "North Hill."

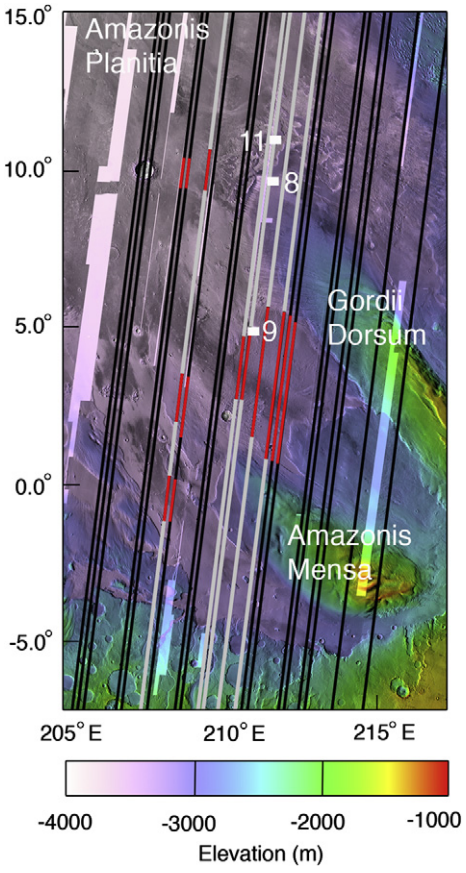

Fig. 4. SHARAD observation ground-tracks across the eastern part of MFF with subsurface interface detections shown in red. The base map is THEMIS daytime infrared with overlaid color MOLA topography. The orbits change from black to red in places where SHARAD detects a subsurface interface. Grey ground tracks correspond to observations shown in Fig. 5. The locations of the HIRISE images shown in Figs. 8, 9 and 11 are indicated with white boxes.

the permittivity (i.e., the real dielectric constant) can be estimated by comparing radargrams with MOLA topography and assuming that the MFF material lies on an constant-elevation extension of nearby plains. The permittivity of the material can be calculated from:

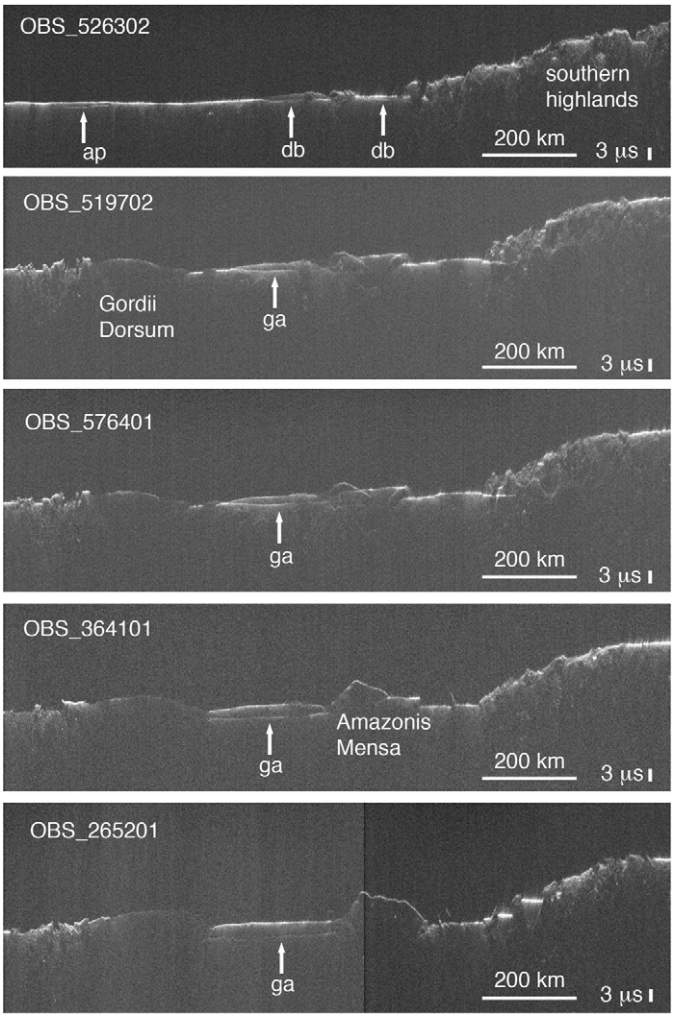

Fig. 5. SHARAD radargrams of deposits in eastern MFF. The radargrams are ordered from west (top) to east (bottom) and are shown with north to the left. Ground tracks are shown in Fig. 4. Subsurface reflectors can be seen between Gordii Dorsum and Amazonis Mensa (arrows marked as ga), as well as in an area near the dichotomy boundary (arrows marked db). Dipping reflectors north of Gordii Dorsum represent contacts between geologic units in southern Amazonis Planitia (arrow marked ap). A scale bar for the time-delay values is shown on the far right or each radargram.

$$\varepsilon' = \left(\frac{c\Delta t}{2h}\right)^2, \tag{1}$$

where h is the height relative to the surrounding plains as measured from MOLA topography and Δt is the two-way time delay between the surface and subsurface echoes measured from the radargram.

In order to illustrate the effects of different values of ε'on the subsurface profiles, we used Eq. (1) to convert time to depth for a range of subsurface ε' values. The depth conversion causes the apparent location of subsurface echoes to migrate upward in proportion to the square root of the real permittivity. Results of these depth conversion adjustments are shown in Fig. 6 for North Hill and Fig. 7 for the eastern MFF between Gordii Dorsum and Amazonis Planitia.

In Fig. 6, a real permittivity value of 3.0 produces a depth profile with a fairly flat interface under both the thin deposit and North Hill. In each Fig. 6 radargram, a black line that connects the plains adjacent to North Hill is shown for comparison with the subsurface echo. A subsurface raised-platform structure is visible beneath the south side of North Hill. Using a real permittivity of 2.0, both subsurface interfaces appear to be concave upward, and

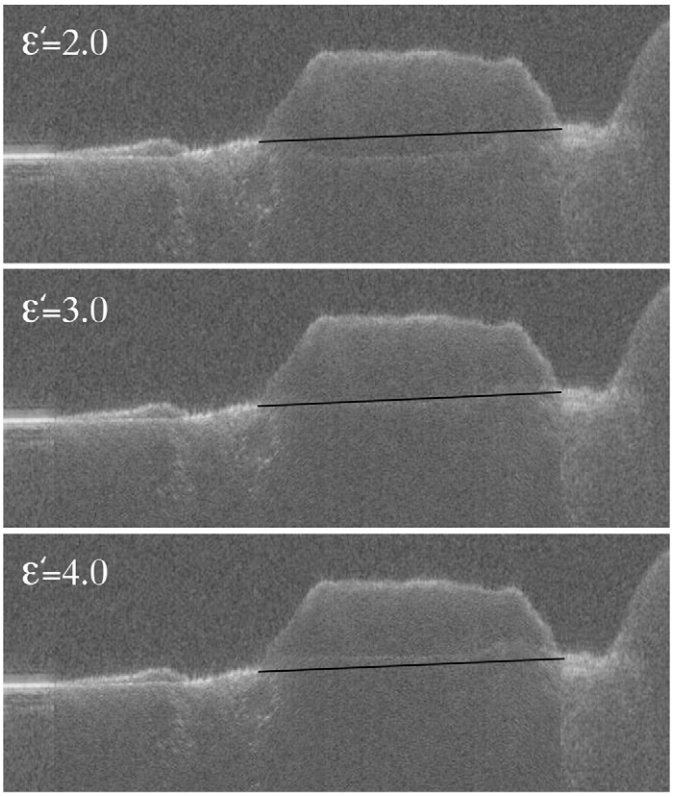

Fig. 6. A portion of SHARAD observation 589803 depth-converted with different values of the permittivity. The full time-delay profile is shown in Fig. 2. A real permittivity value of 3.0 produces a profile where the MFF deposits at North Hill lie on a substrate that gradually increases in elevation to the south (right side of images). Permittivity values that are larger or smaller offset the subsurface interfaces above or below neighboring surface terrain. A black line is shown linking the plains regions on either side of North Hill. For permittivity values of 2.0 or 4.0, the thin deposit to the north has a curved subsurface interface. No reference line is shown for the thin deposit because the line would completely obscure the interface.

the interface has a bowed interface with the plains. For $\varepsilon' = 4.0$, the interface beneath the thin deposit becomes slightly convex, which would imply that the MFF material was deposited on a pre-existing hill. The interface below North Hill is also shallower in the profile than expected for continuity with the surrounding terrain.

Fig. 6 demonstrates that the initial assumption of a flat surface that continues at the same elevation underneath the deposits is not a good approximation for SHARAD. If the subsurface interface under North Hill is at the same elevation as the edge of the plains to the north (on the left side of the images), then the ε' value computed from Eq. (1) is 2.0. This is an extremely low value that produces an unlikely profile where the MFF material is draped over odd-shaped depressions in the plains. Instead, an ε' value of ∼3.0 produces a reasonable geologic interface with a fairly steady upward slope to the south, and with ∼45 m of elevation gain from the plains to the southern edge of North Hill. Permittivity estimates using MARSIS data suffer from this same uncertainty in the subsurface interface depth, but in the MARSIS case the dominant source of error may be the coarser range resolution of the radar. Permittivity estimates from MARSIS data (Watters et al., 2007) include a one-half range bin uncertainty in depth (150 m), and so the small elevation change inferred from the SHARAD data does not substantially change the MARSIS permittivity results for North Hill. It is not possible to compute a more precise North Hill ε' value from the SHARAD data because the depth of the subsurface interface and bench feature are not well-constrained. The actual permittivity could be somewhat higher or lower than 3.

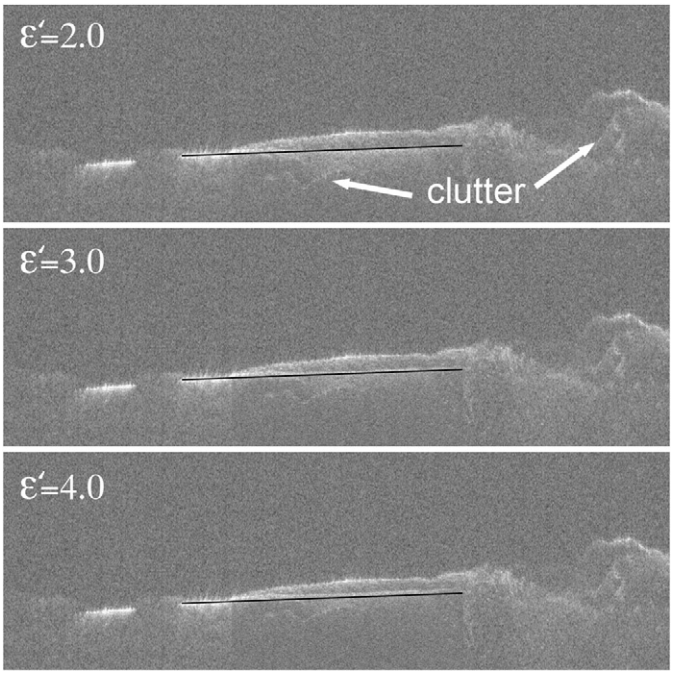

Fig. 7. A portion of SHARAD observation 519702 adjusted for varying values of the permittivity. See Fig. 5 for the full time-delay profile. The slope of the flat plains north of the subsurface interface is extended with a black line. Areas of surface clutter were identified through comparison with simulations and are marked with arrows in the upper ground-track.

The same technique can be used in the eastern parts of the MFF (Fig. 7). In this case, the MFF material appears to lie on a regional slope, regardless of the value selected for the permittivity. The two segments of bright plains reflectors to the north (left) of the subsurface reflector have slightly different slopes. In Fig. 7, the slope of the plains segment nearest the subsurface reflector is continued under the surface with a black line. Maintaining the slope of these plains under the deposit is best done with a permittivity ∼3. For a permittivity value of 4.0, the subsurface interface is noticeably offset to a higher elevation at the boundary between the plains and the deposit. A permittivity of 2.0 places the subsurface interface slightly below the projected slope.

This graphical approach illustrates that a permittivity of ∼3 results in good fits of the subsurface echoes to projections of the surrounding plains, and we use this as an estimate of the bulk permittivity of the MFF as seen by SHARAD. This falls within the 2.9 ± 0.4 range derived by Watters et al. (2007) using MARSIS data. For dry materials, the real part of the permittivity is primarily influenced by density. Pumice, volcanic ash, and tuff have permittivity values between ∼2.5 and 3.5, while basalts have ε' values around 7 to 9 (Campbell and Ulrichs, 1969). Pure water ice has a permittivity of ∼3.1 (Cumming, 1952). As discussed by Watters et al. (2007), it is not possible to uniquely determine the composition of the MFF based on a derived permittivity of 3. However, the low permittivity values inferred from the SHARAD data suggest that the upper few hundred meters of the MFF have a high porosity. One possibility is that these upper layers are low-density, welded or interlocked pyroclastic units.

As a radar wave travels through a deposit, power is lost through attenuation and scattering, resulting in a weaker subsurface echo. Assuming that surface and subsurface roughness are relatively consistent along the orbit track, it is possible to estimate the loss tangent of the material based on the reduction in echo power with round-trip delay (e.g., Campbell et al., 2008; Watters et al., 2007). Using radargrams from across the MFF, with deposit depths ranging from about 0.5 to 2.5 km, Watters et al. (2007) infer a

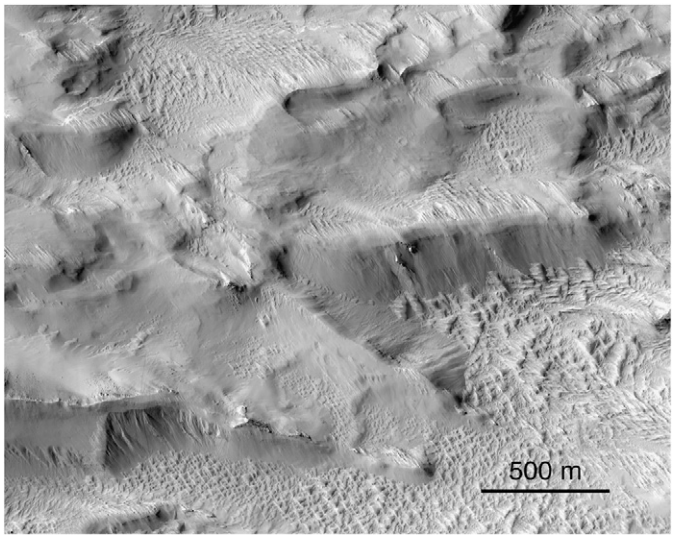

Fig. 8. HIRISE image (TRA_000865_1905) showing the rough surface of Gordii Dorsum and centered at 10.2° N, 211.5° E. The SHARAD surface echo disappears almost completely over this extremely rough terrain.

loss value of 0.0048 ± 0.0024 dB/m ($\tan\delta = 0.002$–0.006) at a frequency of 4 MHz. Although this technique can theoretically be used to derive loss tangents from SHARAD data as well, the interfaces present in the MFF are often diffuse (i.e., the power is spread over several SHARAD range bins). In addition, the surface echo across the MFF deposit is reduced significantly from that of the plains, and both the surface and subsurface echo power vary considerably along track, even as the apparent reflector depth remains fairly constant. These phenomena generate a large amount of scatter in a comparison of echo power versus round-trip time delay. THEMIS and High-Resolution Imaging Science Experiment (HIRISE) images, as well as the variations in SHARAD surface backscatter, reveal that the tens-of-meter-scale surface roughness changes significantly across the MFF, adding an unquantifiable uncertainty to loss tangent measurements derived using radargrams from across the longitudinal extent of the deposit. The MARSIS instrument, with a longer wavelength, is less susceptible to this type of surface clutter. Consequently, the MARSIS radargrams show less variability in surface and subsurface echo power than SHARAD tracks over the same area of the MFF. Although the SHARAD data for the MFF cannot produce a statistically robust estimate of the loss tangent, it is clear from visual inspection of the radargrams that these losses are quite low. For the very thin deposits, such as the low-elevation hills in the west MFF, the subsurface interface generally returns only slightly less echo power than the surface interface.

4. SHARAD echoes and local geology of the Medusae Fossae Formation

The SHARAD radargrams provide insight into the nature of the MFF, particularly when compared with visible and infrared imagery. First, the MFF material is easily penetrable by radar and is rough at the 15-m wavelength scale of SHARAD. The radar echo almost completely disappears across the roughest areas, for example, the northern tip of Gordii Dorsum (Fig. 5). HIRISE images across Gordii Dorsum confirm high surface roughness in areas of low SHARAD backscatter (Fig. 8). Smoother surfaces, such as the region between Gordii Dorsum and Amazonis Mensa, have stronger surface echoes. MARSIS data show similar changes in surface echo

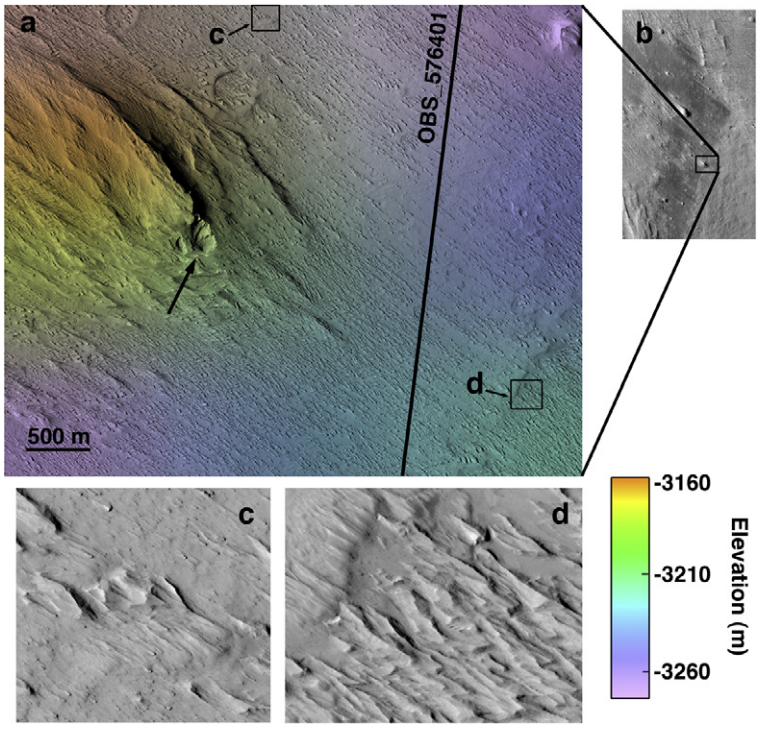

Fig. 9. (a) HIRISE image (PSP_006905_1850) centered at 4.9° N, 210.8° E and showing the edge of a deposit southwest of Gordii Dorsum where SHARAD detects a subsurface interface. Color-stretched MOLA topography is overlaid on the image, with purple representing the lowest elevation values and orange the highest. The SHARAD observation 576401 crosses this image and is marked with a black line. The position of the sub-images in (c) and (d) are marked. A large pit (black arrow) is located near the base of the tall yardangs in the upper left. (b) THEMIS infrared image I03313002 with a box showing the location of the HIRISE image in (a). SHARAD sees through the light-toned deposit. The plains to the north of the deposit show up as dark in the thermal infrared image. The THEMIS image was acquired at 16:38 local time at a solar incidence angle of 66°, where the solar incidence angle is the angle between the Sun and the surface normal. (c) Towards the north and away from the higher elevation deposit, the terrain has fewer yardangs and a larger concentration of big blocks. (d) HIRISE detail of rocks eroding from the friable material. SHARAD does not detect internal layering (see Fig. 5), despite the presence of these darker layers.

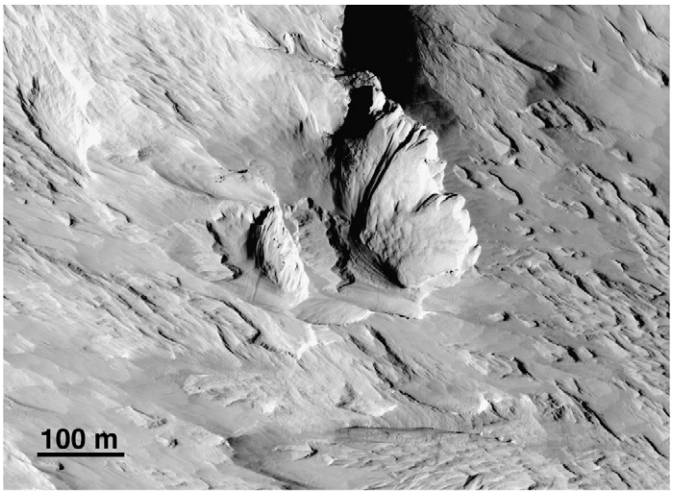

Fig. 10. High-resolution view of the depression near the large yardang in Fig. 9. Slope streaks can be seen descending into the pit and are a useful way to judge the slope directions. The pit is approximately 168 m wide and 250 m long.

strength across the roughest surfaces like Gordii Dorsum, suggesting that surface roughness may play some role in the decreased surface echo power even at very long (50–230 m) wavelengths. The radar-dark behavior of the Stealth area across a wide range of wavelengths is most likely the result of a combination of radar power loss through transmission into a low-permittivity material with no strong internal reflectors and the loss of reflected power due to scattering from surfaces that are rough at wavelength scales ranging from 3 cm through >100 m. The low backscatter at the shorter wavelengths suggests that in most places, the top centimeters of the deposit have few internal reflectors.

There is no clear evidence of internal layering in any of the SHARAD radargrams collected to date across the Medusae Fossae Formation. In the western part of the MFF, the thin deposits penetrated by SHARAD appear to lie atop an extension of the volcanic plains of Elysium Planitia, and the strong permittivity contrast between low-density MFF material and dense volcanic material most likely creates the bright subsurface reflection. There is no evidence for fine-scale internal layering within the ∼580 m North Hill deposit. In the east, the situation is more complex. The area between Gordii Dorsum and Amazonis Mensa consists of stepped layers, evident in MOLA data, that decrease in elevation towards Amazonis Planitia to the northwest with a slope of ∼0.06°. SHARAD sees through only the thinnest part of these layers, which is closest to the plains. Fig. 9a is a HIRISE image of the boundary region where SHARAD is first able to detect an interface beneath this part of the MFF. A THEMIS infrared image (Fig. 9b) shows that SHARAD detects the subsurface interface as the radar moves from a darker surface onto a lighter one that may represent a dustier part of the deposit. This area corresponds to the SHARAD observation 576401 shown in Fig. 5. In the northwestern part of the HIRISE image, the terrain is partially covered by dark blocks (Fig. 9c). Near the center of the image, the ground track crosses onto a low-relief deposit that is easily penetrated by the SHARAD radar. In several places across this deposit, dark blocks can be seen eroding from steep-sided terrain (Fig. 9d); as the material erodes, these blocks may be further exposed to form a surface more like that to the north.

Fig. 9 also shows an unusual oblong depression (Fig. 10) located on the southeast end of a large yardang, just on the edge of the higher-elevation infrared-bright deposit. Blocky material can be seen cascading down the walls of the pit closest to the yardang. The depression does not appear to be an impact structure. If it is an erosional feature, its size would require the removal of a significant amount of material from depth. Instead, the depression may be a pit crater or a relic vent structure, particularly if the MFF is composed of volcanic deposits. If the pit is a volcanic vent, then most of the original surrounding volcanic structure has probably been removed by the wind, perhaps leaving only the portion that includes the large yardang.

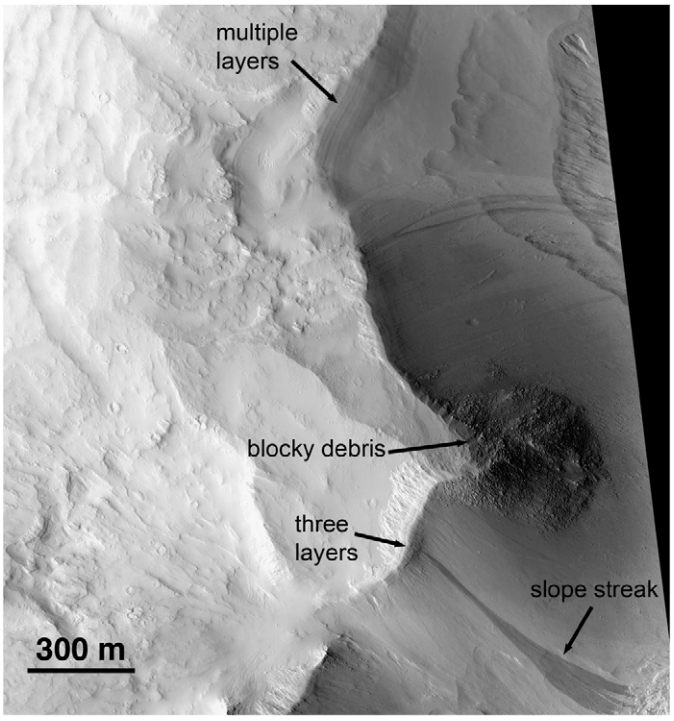

Fig. 11. HIRISE image (PSP_006839_1910) centered at 11.0° N and 211.7° E, showing blocky debris shedding down a slope in eastern MFF. Three layers of more resistant material can be seen along the cliff face in the vicinity of the debris falls. Farther to the north, in the upper-middle part of the image, multiple fine layers can be seen in the cliff face. Slope streaks cover the steep cliff face, highlighting the fine-grained nature of the MFF material. Although the surface to the west is relatively flat compared to other areas of the MFF, SHARAD does not detect these internal layers.

Despite the lack of evidence in the SHARAD data for internal layering within the MFF, evidence of such layering has been documented in MOC, THEMIS, and HIRISE images (e.g., Bradley et al., 2002; Hynek et al., 2003; Zimbelman et al., 1997). Fig. 11 is a HIRISE image of an area north of Gordii Dorsum. In the middle of the image, three dark layers a few meters apart are eroding into blocks that form rock slides along the steep slopes. Farther to the north, multiple fine layers can be seen in the cliffs. The layers are flat and parallel, with no evidence of discontinuities or cross-bedding. Slope streaks are also prevalent in this area, showing the fine-grained nature of the surface materials across most of the area.

There are several reasons why SHARAD might not detect the MFF layers seen in images. Layers could be spaced below the resolution limit of the radar, they may be discontinuous over large regions, or, perhaps most likely, the permittivity contrast between the fine-grained material and the block-forming dark material may not be sufficient to produce a strong reflection. Whatever the reasons for the lack of internal interfaces, it is apparent that the MFF lacks the same type of fine-scale permittivity layering that SHARAD easily detects within the martian polar caps (e.g., Seu et al., 2007b; Phillips et al., 2008). The lack of internal reflectors suggests that the MFF is not an analog to the current martian polar deposits.

Acknowledgments

We thank the SHARAD Operations Center team, including Emanuele Giacomoni, Federica Russo, Marco Cutigni, Oreste Fuga, and Riccardo Mecozzi for their assistance with targeting, calibration, and data processing. We thank the HIRISE and MRO engineering and operations teams for their work in designing, building, and operating the equipment. We are grateful to Fabrizio Bernardini for assistance with SHARAD data processing. Lionel Wilson and an anonymous reviewer provided helpful comments. The Shallow Subsurface Radar (SHARAD) was provided by the Italian Space Agency through a contract with Thales Alenia Space Italia, and it is operated by the INFOCOM Department, University of Rome "La Sapienza." This work was partially supported through a NASA MRO Participating Scientist grant to L.M. Carter.

References

Bradley, B.A., Sakimoto, S.E.H., Frey, H., Zimbelman, J.R., 2002. Medusae Fossae Formation: New perspectives from Mars Global Surveyor. J. Geophys. Res. 107 (E8), doi:10.1029/2001JE001537. 5058.

Campbell, B.A., Carter, L.M., Phillips, R.J., Putzig, N.E., Plaut, J.J., Safaeinili, A., Seu, R., Biccari, D., Orosei, R., 2008. SHARAD radar sounding of Amazonis Planitia. J. Geophys. Res., doi:10.1029/2008JE003177, in press.

Campbell, M., Ulrichs, J., 1969. Electrical properties of rocks and their significance for Lunar radar observations. J. Geophys. Res. 74, 5867–5881.

Christensen, P.R., Jakowsky, B.M., Kieffer, H.H., Malin, M.C., McSween, H.Y., Nealson, K., Mehall, G.L., Silverman, S.H., Ferry, S., Caplinger, M., Ravine, M., 2004. The Thermal Emission Imaging System (THEMIS) for the Mars 2001 Odyssey Mission. Space Sci. Rev. 110, 85–130.

Crown, D.A., Greeley, R., 1993. Volcanic geology of Hadriaca Patera and the Eastern Hellas region on Mars. J. Geophys. Res. 98, 3431–3451.

Cumming, W.A., 1952. The dielectric properties of ice and snow at 3.2 centimeters. J. Appl. Phys. 23, 768–773.

Edgett, K.S., Malin, M.C., 2000. A meter-scale view of the Mars radar "Stealth" Southwest Tharsis. Lunar Planet. Sci. 31. Abstract #1065.

Edgett, K.S., Butler, B.J., Zimbelman, J.R., Hamilton, V.E., 1997. Geologic context of the Mars radar "Stealth" region in southwestern Tharsis. J. Geophys. Res. 102, 21545–21567.

Fagents, S.A., Wilson, L., 1996. Numerical modeling of ejecta dispersal from transient volcanic explosions on Mars. Icarus 123, 284–295.

Glaze, L.S., Baloga, S.M., 2002. Volcanic plume heights on Mars: Limits of validity for convective models. J. Geophys. Res. 107 (E10), doi:10.1029/2001JE001830. 5086.

Greeley, R., Crown, D.A., 1990. Volcanic geology of Tyrrhena Patera, Mars. J. Geophys. Res. 95, 7133–7149.

Harmon, J.K., Arvidson, R.E., Guinness, E.A., Campbell, B.A., Slade, M.A., 1999. Mars mapping with delay-Doppler radar. J. Geophys. Res. 104, 14065–14090.

Head, J.W., Kreslavsky, M., 2004. Medusae Fossae Formation: Ice-rich airborne dust deposited during periods of high obliquity? Lunar Planet. Sci. 35. Abstract #1635.

Hynek, B.M., Phillips, R.J., Arvidson, R.E., 2003. Explosive volcanism in the Tharsis region: Global evidence in the martian geologic record. J. Geophys. Res. 108 (E9), doi:10.1029/2003JE002062. 5111.

Mouginis-Mark, P.J., 2002. Prodigious ash deposits near the summit of Arsia Mons volcano, Mars. Geophys. Res. Lett. 29 (16), doi:10.1029/2002GL015296. 1768.

Mouginis-Mark, P.J., Wilson, L., Zimbelman, J.R., 1988. Polygenic eruptions on Alba Patera, Mars. Bull. Volcanol. 50, 361–379.

Muhleman, D.O., Butler, B.J., Grossman, A.W., Slade, M.A., 1991. Radar images of Mars. Science 253, 1508–1513.

Muhleman, D.O., Grossman, A.W., Butler, B.J., 1995. Radar investigations of Mars, Mercury, and Titan. Annu. Rev. Earth Planet. Sci. 23, 337–374.

Phillips, R.J., Zuber, M.T., Smrekar, S.E., Mellon, M.T., Head, J.W., Tanaka, K.L., Putzig, N.E., Milkovich, S.M., Campbell, B.A., Plaut, J.J., Safaeinili, A., Seu, R., Biccari, D., Carter, L.M., Picardi, G., Orosei, R., Mohit, P.S., Heggy, E., Zurek, R.W., Egan, A.F., Giacomoni, E., Russo, F., Cutigni, M., Pettinelli, E., Holt, J.W., Leuschen, C.J., Marinangeli, L., 2008. Mars North Polar deposits: Stratigraphy, age, and geodynamical response. Science 320, 1182–1185.

Picardi, G., Plaut, J.J., Biccari, D., Bombaci, O., Calabrese, D., Cartacci, M., Cicchetti, A., Clifford, S.M., Edenhofer, P., Farrell, W.M., Federico, C., Frigeri, A., Gurnett, D.A., Hagfors, T., Heggy, E., Herique, A., Huff, R.L., Ivanov, A.B., Johnson, W.T.K., Jordan, R.L., Kirchner, D.L., Kofman, W., Leuschen, C.J., Nielsen, E., Orosei, R., Pettinelli, E., Phillips, R.J., Plettemeier, D., Safaeinili, A., Seu, R., Stofan, E.R., Vannaroni, G., Watters, T.R., Zampolini, E., 2005. Radar soundings of the subsurface of Mars. Science 310, 1925–1928.

Robinson, M.S., Mouginis-Mark, P.J., Zimbelman, J.R., Wu, S.S.C., Ablin, K.K., Howington-Kraus, A.E., 1993. Chronology, eruption duration, and atmospheric contribution of the martian volcano Apollinaris Patera. Icarus 104, 301–323.

Safaeinili, A., Kofman, W., Mouginot, J., Gim, Y., Herique, A., Ivanov, A.B., Plaut, J.J., Picardi, G., 2007. Estimation of the total electron content of the martian ionosphere using radar sounder echoes. Geophys. Res. Lett. 34, doi:10.1029/2007GL032154. L23204.

Schultz, P., Lutz, A.B., 1988. Polar wandering of Mars. Icarus 73, 91–141.

Seu, R., Biccari, D., Orosei, R., Lorenzoni, L.V., Phillips, R.J., Marinangeli, L., Picardi, G., Masdea, A., Zampolini, E., 2004. SHARAD: The MRO 2005 shallow radar. Planet. Space Sci. 52, 157–166.

Seu, R., Phillips, R.J., Biccari, D., Orosei, R., Masdea, A., Picardi, G., Safaeinili, A., Campbell, B.A., Plaut, J.J., Marinangeli, L., Smrekar, S.E., Nunes, D.C., 2007a. SHARAD sounding radar on the Mars Reconnaissance Orbiter. J. Geophys. Res. 112, doi:10.1029/2006JE002745. E05S05.

Seu, R., Phillips, R.J., Alberti, G., Biccari, D., Bonaventura, F., Bortone, M., Calabrese, D., Campbell, B.A., Cartacci, M., Carter, L.M., Catallo, C., Croce, A., Croci, R., Cutigni, M., Di Placido, A., Dinardo, S., Federico, C., Flamini, E., Fois, F., Frigeri, A., Fuga, O., Giacomoni, E., Gim, Y., Guelfi, M., Holt, J.W., Kofman, W., Leuschen, C.J., Marinangeli, L., Marras, P., Masdea, A., Mattei, S., Mecozzi, R., Milkovich, S.M., Morlupi, A., Mouginot, J., Orosei, R., Papa, C., Paternò, T., Persi del Marmo, P., Pettinelli, E., Pica, G., Picardi, G., Plaut, J.J., Provenziani, M., Putzig, N.E., Russo, F., Safaeinili, A., Salzillo, G., Santovito, M.R., Smrekar, S.E., Tattarletti, B., Vicari, D., 2007b. Accumulation and erosion of Mars' South Polar layered deposits. Science 317, 1715–1718.

Tanaka, K.L., 2000. Dust and ice deposition in the martian record. Icarus 144, 254–266.

Tanaka, K.L., Skinner, J.A., Hare, T.M., 2005. Geologic map of the northern plains of Mars. US Geol. Surv. Sci. Inv. Map 2888.

Watters, T.R., Campbell, B.A., Carter, L.M., Leuschen, C.J., Plaut, J.J., Picardi, G., Orosei, R., Safaeinili, A., Clifford, S.M., Farrell, W.M., Ivanov, A.B., Phillips, R.J., Stofan, E.R., 2007. Radar sounding of the Medusae Fossae Formation, Mars: Equatorial ice or dry, low-density deposits? Science 318, 1125–1128.

Wilson, L., Head, J.W., 2007. Explosive volcanic eruptions on Mars: Tephra and accretionary lapilli formation, dispersal and recognition in the geologic record. J. Volcanol. Geotherm. Res. 163, 83–97.

Zimbelman, J.R., Crown, D.A., Grant, J.A., Hooper, D.M., 1997. The Medusae Fossae Formation, Amazonis Planitia, Mars: Evaluation of proposed hypothesis of origin. Lunar Planet. Sci. 28. Abstract #1482.